Available online at www.sciencedirect.com

ScienceDirect

Ceramics International 40 (2014) 3667–3677

CERAMICS INTERNATIONAL

www.elsevier.com/locate/ceramint

Effects of Al_2O_3 and NbC additives on the microstructure and mechanical properties of TiB_2–TiC composite ceramic cutting tool materials

Bin Zou[a,b,*], Chuanzhen Huang[a,b], Wenbin Ji[a,b], Shasha Li[c]

[a]Centre for Advanced Jet Engineering Technologies (CaJET), School of Mechanical Engineering, Shandong University, 17923 Jing Shi Road, Jinan 250061, PR China

[b]Key Laboratory of High Efficiency and Clean Mechanical Manufacture (Shandong University), Ministry of Education, PR China

[c]Shandong Special Equipment Inspection Institute, Jinan 250013, PR China

Received 31 August 2013; received in revised form 13 September 2013; accepted 13 September 2013
Available online 27 September 2013

Abstract

A study of the effects of Al_2O_3 and NbC additives on the microstructure and mechanical properties of TiB_2–TiC composite ceramic cutting tool materials is presented. The relations of the room temperature and high-temperature mechanical properties to the microstructure of the composite were investigated. The Al_2O_3 additive was determined to slightly increase the flexural strength and fracture toughness of the composite at room temperature and significantly increase the flexural strength of the composite at high temperatures. The superfine NbC additive improved the room-temperature flexural strength of the composite by approximately 30%. The microstructure was refined, and the resultant mechanical properties were improved if Al_2O_3 and NbC were added to the composite together. The flexural strength of the TiB_2–TiC + Al_2O_3 + NbC composite material still exceeded 500 MPa at 800 °C, which can meet the demands of cutting tool materials. The quick degradation of the high-temperature flexural strength of the composite above 800 °C was mainly due to the softening of Ni binder phase.

Keywords: A. Sintering; B. Microstructure; C. Mechanical property; E. Cutting tools

1. Introduction

Because cutting tools are used in undesirable environments during the machining of metals, the tool materials must have excellent mechanical properties at room temperature and high temperatures. Additives can change the mechanical properties of the tool materials. Al_2O_3, TiC and TiB_2 phases are perfect candidates for tool materials due to their high hardness and thermal stabilities [1]. Vallauri et al. [2] found that the beneficial coherency between (111)TiC and (0001)TiB_2 interfaces contributed to an improvement of the toughness of TiC–TiB_2 composite materials. However, the high melting points of phases are the biggest obstacle to the fabrication of TiC–TiB_2 composite ceramic cutting tool materials. Gu et al. [3] found that Al_2O_3 could improve the density of TiB_2-based composite ceramic and reduce its sintering temperature. Zou et al. [4] attempted to fabricate a TiB_2–TiC + Al_2O_3 composite powder via a reaction in an Al–TiO_2–B_4C system. However, this attempt was unsuccessful due to challenges in removing the impurities from the composite. Our previous studies [5–6] demonstrated that the TiB_2–TiC composite material was very hard, but its flexural strength was low unless the content of the metal binder phase exceeded 10 wt%. The addition of the metal binder phase rapidly reduces the red-hardness of the tool materials. More importantly, the grain size of the starting powder significantly influences the mechanical properties of the composite. Because the commercially available TiB_2 starting powder usually has a large grain size, the grain size of TiB_2-based composite materials is usually larger after sintering. A larger grain size can cause a non-homogenous microstructure, which hinders the improvement of the mechanical properties of the TiB_2-based composite material.

*Corresponding author at: Centre for Advanced Jet Engineering Technologies (CaJET), School of Mechanical Engineering, Shandong University, 17923 Jing Shi Road, Jinan 250061, PR China. Tel.: +86 531 88396913; fax: +86 531 88396912.

E-mail addresses: zb78@sdu.edu.cn, zou20011110@163.com (B. Zou).

0272-8842/$ - see front matter © 2013 Elsevier Ltd and Techna Group S.r.l. All rights reserved.
http://dx.doi.org/10.1016/j.ceramint.2013.09.058

Many studies have found that NbC can control the abnormal grain growth of Ti(CN) metal ceramic. Wang et al. [7] reported that a 5 wt% NbC additive improved the densification and refined the microstructure of Ti(C,N)-based composite materials. Few studies have investigated the effects of superfine NbC additive on the microstructure and mechanical properties of TiB_2–TiC composite materials. Raju et al. [8] even found that the strength of TiB_2-based composite materials could be increased with the temperature. This report implies that the TiB_2-based composite materials are promising cutting tool materials because the high-temperature strength is important to the performance of the tool materials. Yin et al. [9] found that the flexural strength of Al_2O_3-based composite materials was approximately 600 MPa, which indicated that the Al_2O_3-based composite materials can meet the demands of the cutting tool materials.

In our work, Al_2O_3 and superfine NbC were added to the TiB_2–TiC mixed crystal powder, and TiB_2–TiC, TiB_2–TiC + Al_2O_3 and TiB_2–TiC + Al_2O_3 + NbC composite materials were then prepared via hot-pressing under a vacuum atmosphere. The effects of Al_2O_3 and NbC additives on the microstructure and mechanical properties of the composites were investigated. The room temperature and high-temperature mechanical properties and their relations to various microstructures are discussed.

2. Experimental methods

The starting material was a commercially available TiB_2–TiC mixed powder (TiB_2 = 75 wt%, TiC = 25 wt%, an average grain size of 1.5 μm). Nickel nano-powder of 99.9% purity with an average grain size of 80 nm was used as the sintering binder phase. The Al_2O_3 and superfine NbC powders of > 99.9% purity with average grain sizes of 0.5 μm and 0.8 μm, respectively, were used as the additives. The composites were prepared by four steps. First, TiB_2–TiC and Al_2O_3 powders were ball-milled in ethanol for 48 h to crush the large particles. They were then dried in a vacuum dry evaporator. Second, TiB_2–TiC, Al_2O_3, NbC and Ni powders were mixed in ethanol for 48 h in a polyethylene jar (their composition ratios can be seen in Table 1). Third, the mixed power was dried in a vacuum dry evaporator. It was then sieved through a 200-mesh sieve for further use. Fourth, the dried powder was sintered via hot-pressing in a graphite die under a vacuum atmosphere at a temperature of 1650 °C, with a holding time of 75 min at 30 MPa of pressure.

Table1
Composition ratios of composite ceramic cutting tool materials (wt%).

Composite material	TiB_2–TiC	Al_2O_3	Al_2O_3	Ni
TiB_2–TiC	93.5	–	–	6.5
TiB_2–TiC + Al_2O_3	75.5	18.0	–	6.5
TiB_2–TiC + Al_2O_3 + NbC	72.3	18.0	3.2	6.5

The dense hot-pressed disks were cut into bars via electrospark wire-electrode cutting, and the bars were ground into starting specimens of 3 mm × 4 mm × 40 mm, and the starting specimens were polished into the tested specimens with a diamond paste. The edges of the tested specimens were chamfered to eliminate some machining flaws that could act as the fracture origins. The room temperature flexural strength was measured using a three-point bending tester (Model WD-10, China) with a span of 20 mm at a loading velocity of 0.5 mm/min. The high-temperature flexural tests were carried out with a span of 20 mm and a loading velocity of 0.5 mm/min at temperatures ranging from 600 to 1000 °C in ambient air by a special machine equipped with a high-temperature controlling system (Istron8801, British). The Vickers hardness was measured on the polished surface using a Vickers diamond pyramid indenter (Model 120, China) with a load of 196 N and a loading duration of 15 s. The fracture toughness was determined using the equation method proposed by Evans [10]. The microstructure of the composite was observed by scanning electron microscopy, energy-dispersive spectrometry (SEM and EDS, SUPRA55, Germany) and X-ray diffraction analysis with copper Kα radiation (XRD, D8, Germany). Scanning transmission electron microscopy (STEM) and transmission electron microscopy (TEM, JEM-2100F, Japan) were also used to observe the microstructure of specimens in more detail, and the samples for STEM were prepared by the following methods: cutting, grinding, dimpling and ion beam thinning.

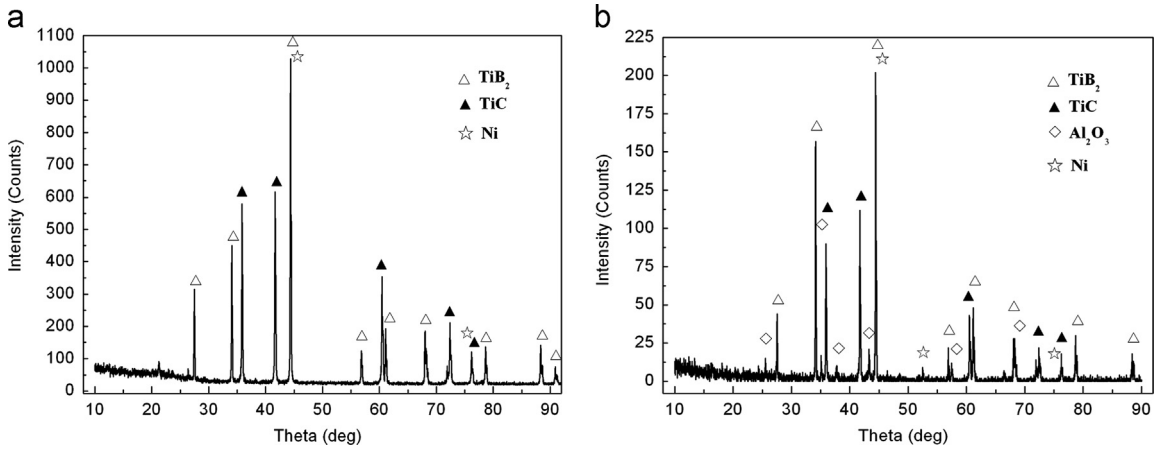

Fig. 1. XRD patterns of the (a) TiB_2–TiC and (b) TiB_2–TiC + Al_2O_3 composite materials.

3. Results and discussion

3.1. Microstructure

Fig. 1 shows the XRD patterns of the TiB_2–TiC and TiB_2–TiC + Al_2O_3 composite materials. According to the XRD cards [11], the TiB_2–TiC composite material mainly consisted of TiB_2 and TiC phases. Apart from the TiB_2 and TiC phases, the main peaks of an Al_2O_3 phase were clearly detected in the XRD pattern of the TiB_2–TiC + Al_2O_3 composite material. New phases were not found in the TiB_2–TiC + Al_2O_3 composite material, indicating that additional reactions did not occur when Al_2O_3 was added to the composite. Fig. 2 shows the SEM and EDS micrographs of the TiB_2–TiC and TiB_2–TiC + Al_2O_3 composite materials. Two predominant phases were observed in the TiB_2–TiC composite material, but the TiB_2–TiC + Al_2O_3 composite material was found to mainly consist of three phases (see Fig. 2(a) and (b)). The EDS patterns reveals that the grey and white phases consisted of TiB_2 and TiC in the TiB_2–TiC composite material (see Fig. 2 (c) and (d)), and the white, grey and dark phases in the TiB_2–TiC + Al_2O_3 composite material corresponded to TiC, TiB_2

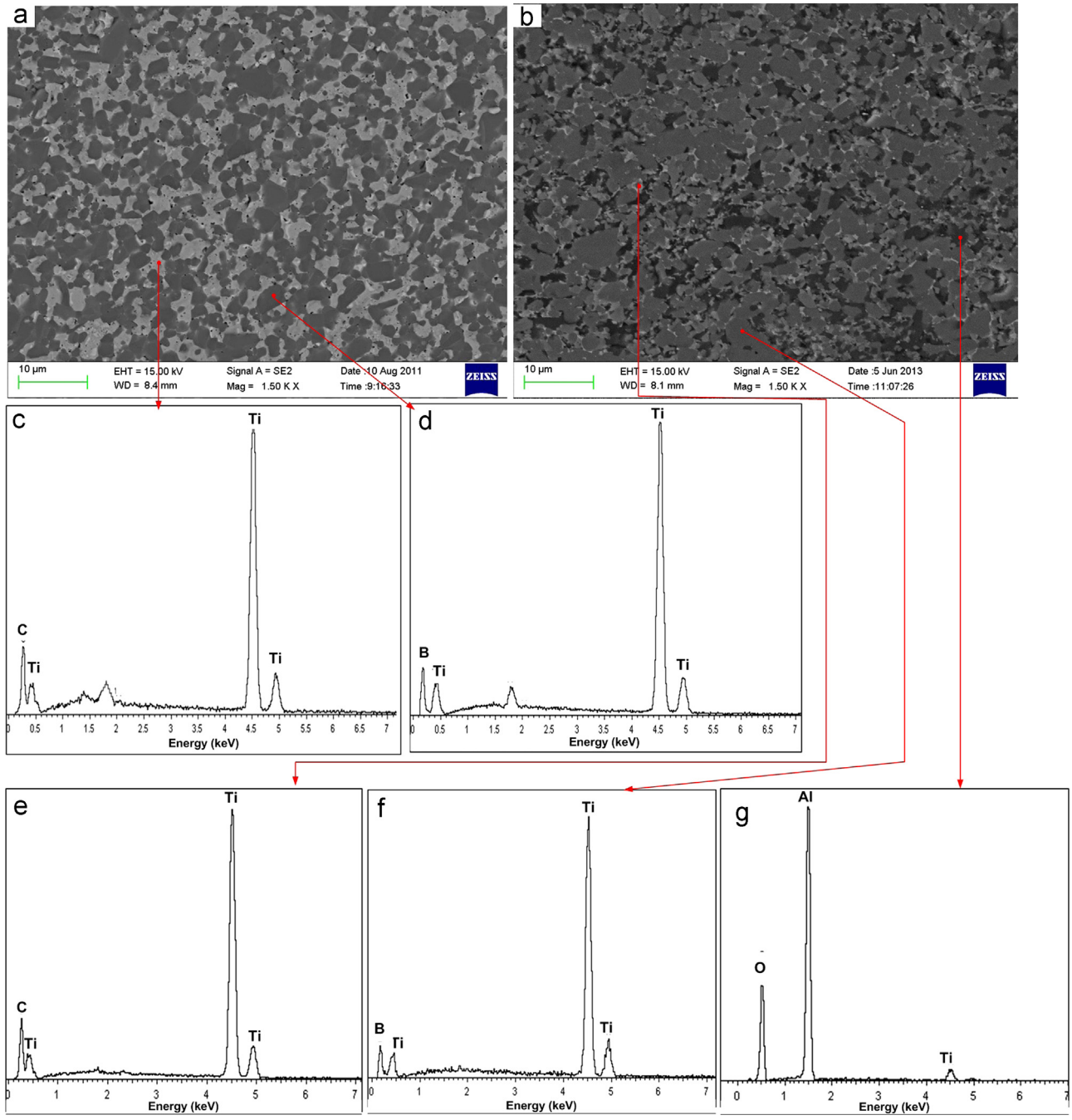

Fig. 2. SEM and EDS micrographs of the TiB_2–TiC and TiB_2–TiC + Al_2O_3 composite materials. EDS micrographs indicate that the TiB_2–TiC composite material mainly included the TiB_2 and TiC phases; the TiB_2–TiC + Al_2O_3 composite material mainly included TiB_2, TiC and Al_2O_3 phases.

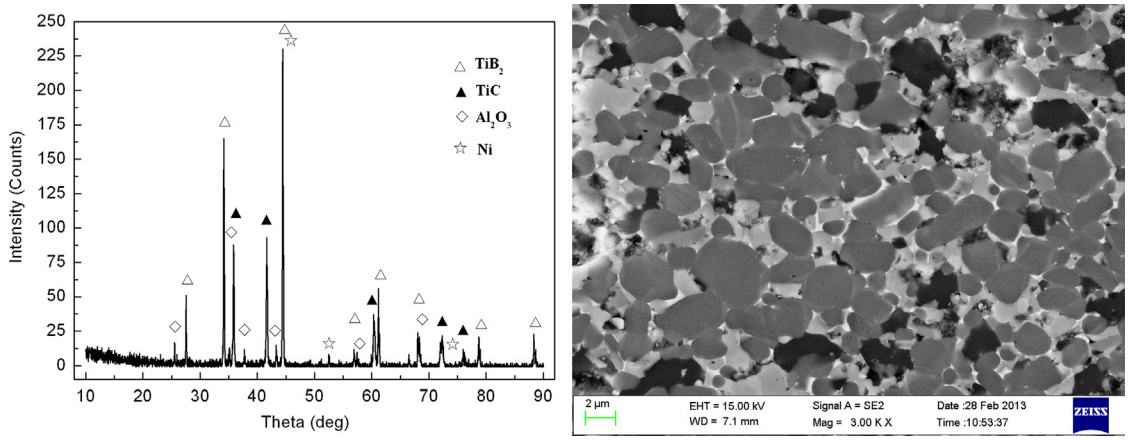

Fig. 3. XRD pattern and SEM micrograph of the polished surface of the TiB_2–$TiC+Al_2O_3+NbC$ composite material. The main phases of the TiB_2–$TiC+Al_2O_3$ and TiB_2–$TiC+Al_2O_3+NbC$ composite materials did not significantly differ. However, grains of the TiB_2–$TiC+Al_2O_3+NbC$ composite material were refined.

and Al_2O_3 (see Fig. 2(e)–(g)). The results identified by the SEM and EDS micrographs were consistent with the XRD patterns. The Al_2O_3 grains were homogeneously distributed among the TiB_2 and TiC grains, and agglomerated Al_2O_3 grains were not observed in the TiB_2–$TiC+Al_2O_3$ composite material. The TiB_2–$TiC+Al_2O_3$ composite materials had larger TiB_2 grains than the TiB_2–TiC composite material. However, the TiC grains were finer in the TiB_2–$TiC+Al_2O_3$ than in the TiB_2–TiC composite materials because several TiC grains gathered in the latter, indicating that the addition of Al_2O_3 positively affected the distribution of TiC grains.

To homogenise and refine the microstructure, some superfine NbC was added to the TiB_2–$TiC+Al_2O_3$ composite material. The XRD pattern and SEM micrograph of the TiB_2–$TiC+Al_2O_3+NbC$ composite material are shown in Fig. 3. The TiB_2–$TiC+Al_2O_3+NbC$ composite material was found to be dominantly comprised of the TiB_2, TiC and Al_2O_3 phases, which were similar to the TiB_2–$TiC+Al_2O_3$ material. The TiB_2 grains exhibited two morphologies in the TiB_2–$TiC+Al_2O_3+NbC$ composite material: one was an elongated shape and the other was an equiaxed shape. The percentage of the equiaxed TiB_2 grains was higher than that of the elongated TiB_2 grains. However, the aspect ratios of the elongated TiB_2 grains were not very large. Furthermore, the TiB_2 grains were finer in the TiB_2–$TiC+Al_2O_3+NbC$ than in the TiB_2–$TiC+Al_2O_3$ composite materials, indicating that the addition of superfine NbC refined the microstructure of the composite.

STEM micrographs of the TiB_2–$TiC+Al_2O_3$ and TiB_2–$TiC+Al_2O_3+NbC$ composite materials are shown in Figs. 4 and 5 respectively. The Al_2O_3 grains were embedded among the TiB_2 and TiC grains, and the Al_2O_3 grains did not aggregate in these two composite materials. Some of the Ni binder phase was distributed on the grain boundaries among the TiB_2, TiC and Al_2O_3 grains, indicating that the Ni binder phase could wet the grains well in the composite. Some of the Ni binder phase also collected on the triple junctions among the grains. In the TiB_2–$TiC+Al_2O_3+NbC$ composite material, a high concentration of the Ti element colocalised with the Nb element. More importantly, Nb was not detected where Ti was absent, which implied that the Nb was incorporated into the phases containing the Ti. Furthermore, the distributions of the Nb, B and C indicate that most of Nb entered the TiC phase, and the remaining Nb was integrated with the TiB_2 phase. The good matches among the NbC, TiC and TiB_2 phases changed the grain growth in the composite. The grain growth of the cermet material proceeded with the dissolution and re-precipitation in the Ni liquid binder by Ostwald ripening [7]. In the TiB_2–TiC composite material, the smaller TiB_2 grains were dissolved in the liquid Ni binder phase and re-precipitated on the larger grains. However, this dissolution and re-precipitation process was changed by the addition of superfine NbC. The superfine NbC additive dissolved rapidly in the Ni liquid phase due to its smaller grains and higher chemical activities. Thus, the Nb was more concentrated in the liquid phase, which decelerated the dissolution of the Ti element into the liquid phase. The lower concentration of the Ti element in the liquid phase reduced the growth rate of TiB_2 grains. Therefore, the microstructure of the TiB_2–$TiC+Al_2O_3+NbC$ composite material was refined by the addition of the superfine NbC.

3.2. Mechanical properties

The room temperature mechanical properties of three composite materials are listed in Table 2. The TiB_2–TiC composite material exhibited a flexural strength of 870 MPa, fracture toughness of 7.30 MPa $m^{1/2}$ and hardness of 21.42 GPa. When Al_2O_3 was added, the flexural strength and fracture toughness of the composite slightly increased to 962 MPa and 8.00 MPa $m^{1/2}$, respectively, while the hardness decreased to 20.00 GPa. When the Al_2O_3 and superfine NbC were added together, the flexural strength, fracture toughness and hardness of the composite were 1202 MPa, 8.13 MPa $m^{1/2}$ and 20.73 GPa, respectively. The flexural strength of the TiB_2–$TiC+Al_2O_3+NbC$ composite material was improved by approximately 30% compared with that of the TiB_2–TiC composite material. The improvement in the flexural strength of the composite was related to the refinement of the microstructure. The addition of Al_2O_3 halted

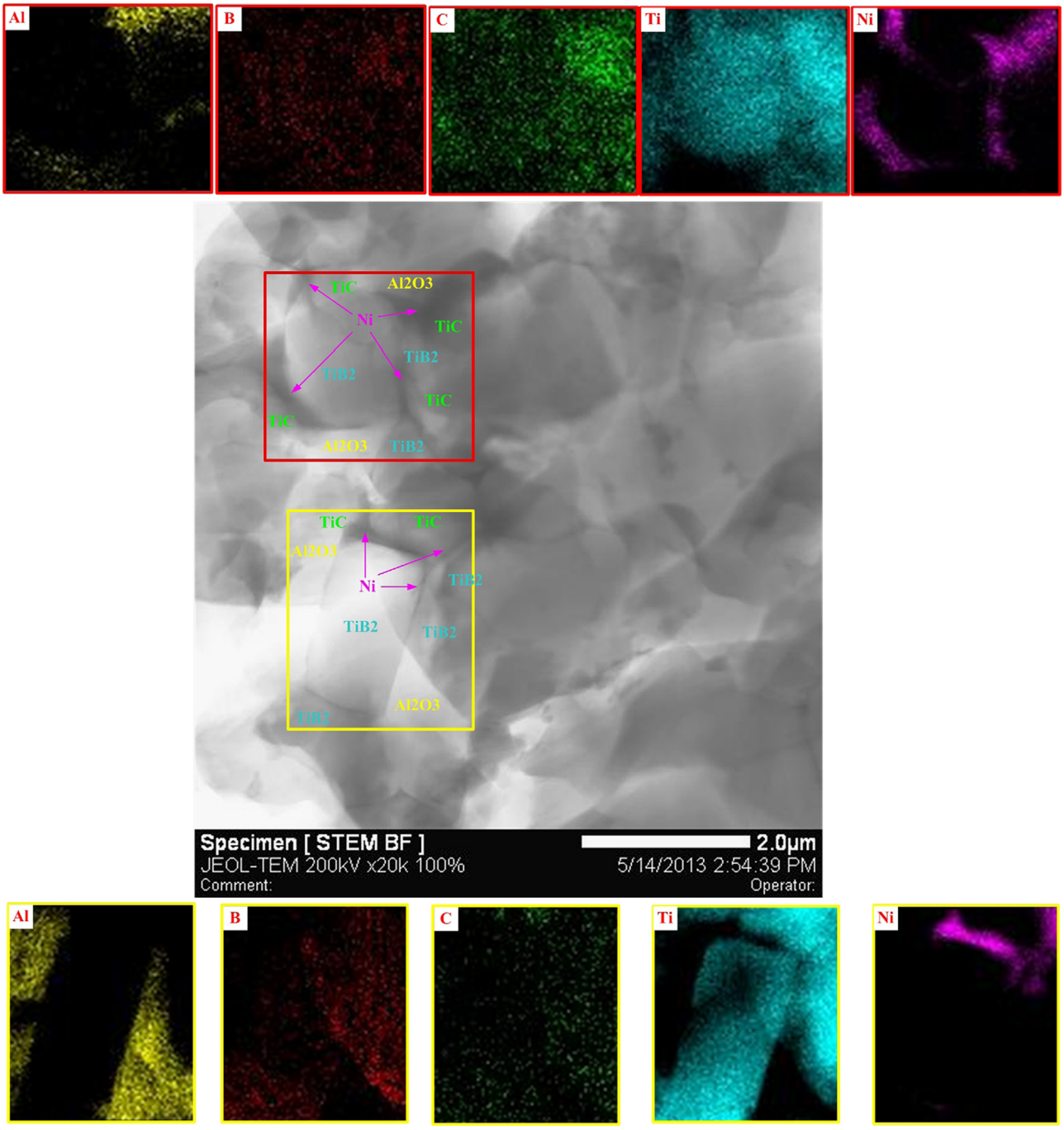

Fig. 4. STEM and EDS micrographs of the TiB_2–TiC + Al_2O_3 composite material. The distributions of five elements (Al, B, C, Ti and Ni) were detected by the area EDS analysis, and their corresponding phases were marked in the STEM micrograph.

the agglomeration of TiC grains but caused a further growth of the TiB_2 grains (see Fig. 2). The agglomerated TiC grains were subject to failure due to their flaws, and the bigger TiB_2 grains were prone breakage due to their brittle nature. Therefore, the TiB_2–TiC + Al_2O_3 composite material exhibited a slightly higher flexural strength and fracture toughness than the TiB_2–TiC composite material. However, the addition of NbC inhibited the growth of TiB_2 grains, which significantly improved the flexural strength of the composite.

Fig. 6 show SEM micrographs of the fracture surfaces of the TiB_2–TiC, TiB_2–TiC + Al_2O_3 and TiB_2–TiC + Al_2O_3 + NbC composite materials. Many grains were found to have exited the grain boundaries on the fracture surface of the TiB_2–TiC composite material (see the green arrows in Fig. 6(a)). A fractured terrace was observed on the fracture surface of the TiB_2–TiC + Al_2O_3 composite material (see the red circle in Fig. 6(b)), which benefitted the mechanical properties. However, some of the bigger grains were cleaved, which adversely affected the mechanical properties due to the brittle nature of the bigger grains (see the yellow arrows in Fig. 6(b)). The fracture surface of the TiB_2–TiC + Al_2O_3 + NbC composite material was very rough and uneven (see Fig. 6(c)), and

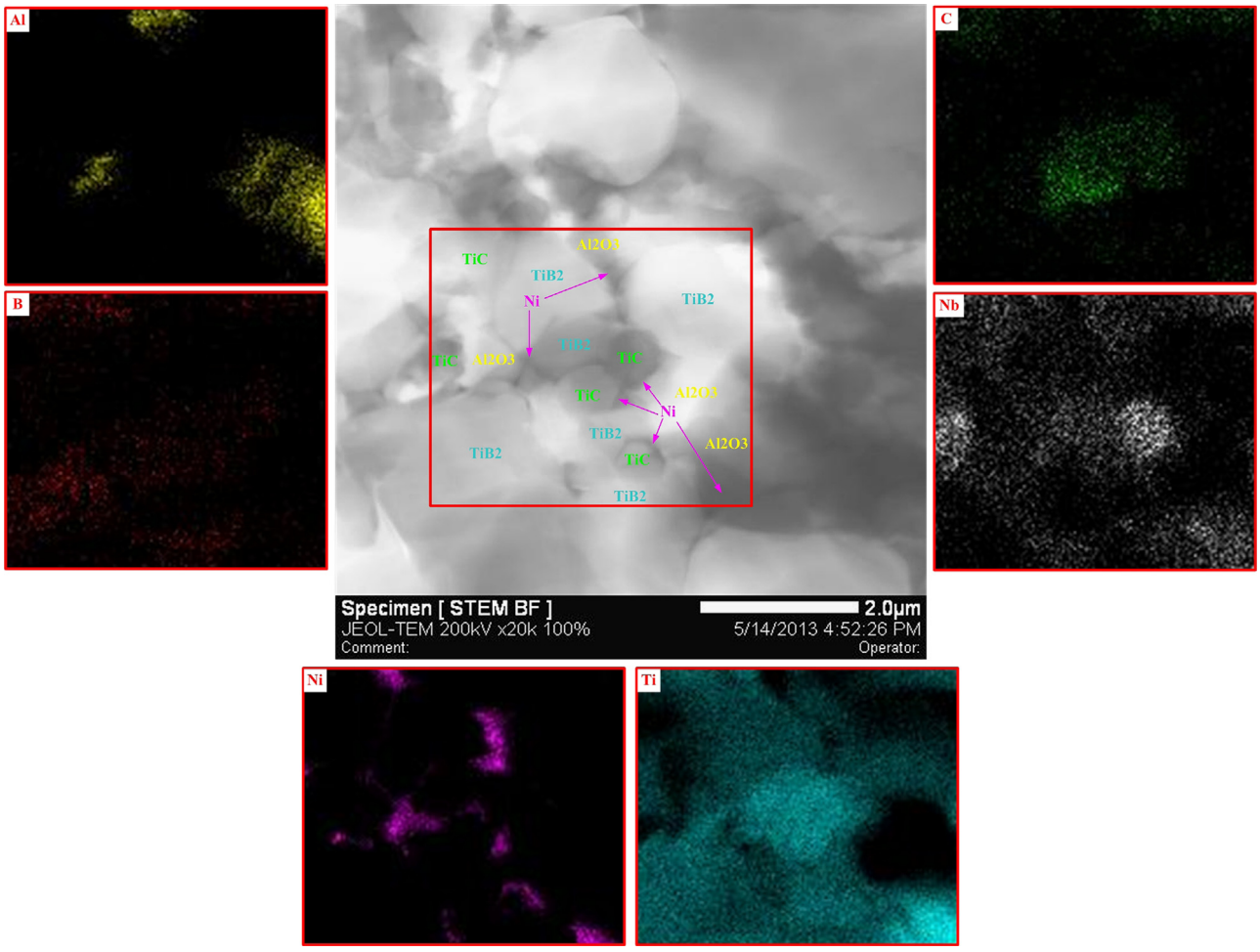

Fig. 5. STEM and EDS micrographs of the TiB_2–TiC + Al_2O_3 + NbC composite material. The distributions of six elements (Al, B, C, Ti, Ni and Nb) were detected by the area EDS analysis, and their corresponding phases were marked in the STEM micrograph.

Table 2
Room-temperature mechanical properties of three composite ceramic cutting tool materials.

Composite materials	Room-temperature mechanical properties		
	Flexural strength (MPa)	Fracture toughness (MPa $m^{1/2}$)	Hardness (GPa)
TiB_2–TiC	870	7.30	21.42
TiB_2–TiC + Al_2O_3	962	8.00	20.00
TiB_2–TiC + Al_2O_3 + NbC	1202	8.13	20.73

some morphologies seemed to experience a few plastic deformations (see the blue circles in Fig. 6(c)). Furthermore, the homogenous Ni phase in the composite, in particular the Ni phase in the triple junctions among grains, could prevent the grains from being drawn and generating plastic deformations. Thus, the flexural strength of the TiB_2–TiC + Al_2O_3 + NbC composite material was primarily significantly improved due to the finer grains and homogenous Ni binder phase in the microstructure.

The flexural strength at the different temperatures was investigated to explain the fracture mechanism of the composite. Fig. 7 shows the flexural strength of the TiB_2–TiC, TiB_2–TiC + Al_2O_3 and TiB_2–TiC + Al_2O_3 + NbC composite materials at room temperature and 600 °C. The flexural strength of all composites decreased when the temperature was increased from room temperature to 600 °C. This finding was not consistent with that by Raju [8], who demonstrated that the flexural strength of the TiB_2-based composite positively correlated with the temperature. Compared with the room-temperature flexural strength, the flexural strength of the TiB_2–TiC composite material was reduced by approximately 50% at 600 °C, and the flexural strength of the TiB_2–TiC + Al_2O_3 composite material was reduced by 30% at 600 °C, which indicates that the Al_2O_3 additive decelerated the degradation of

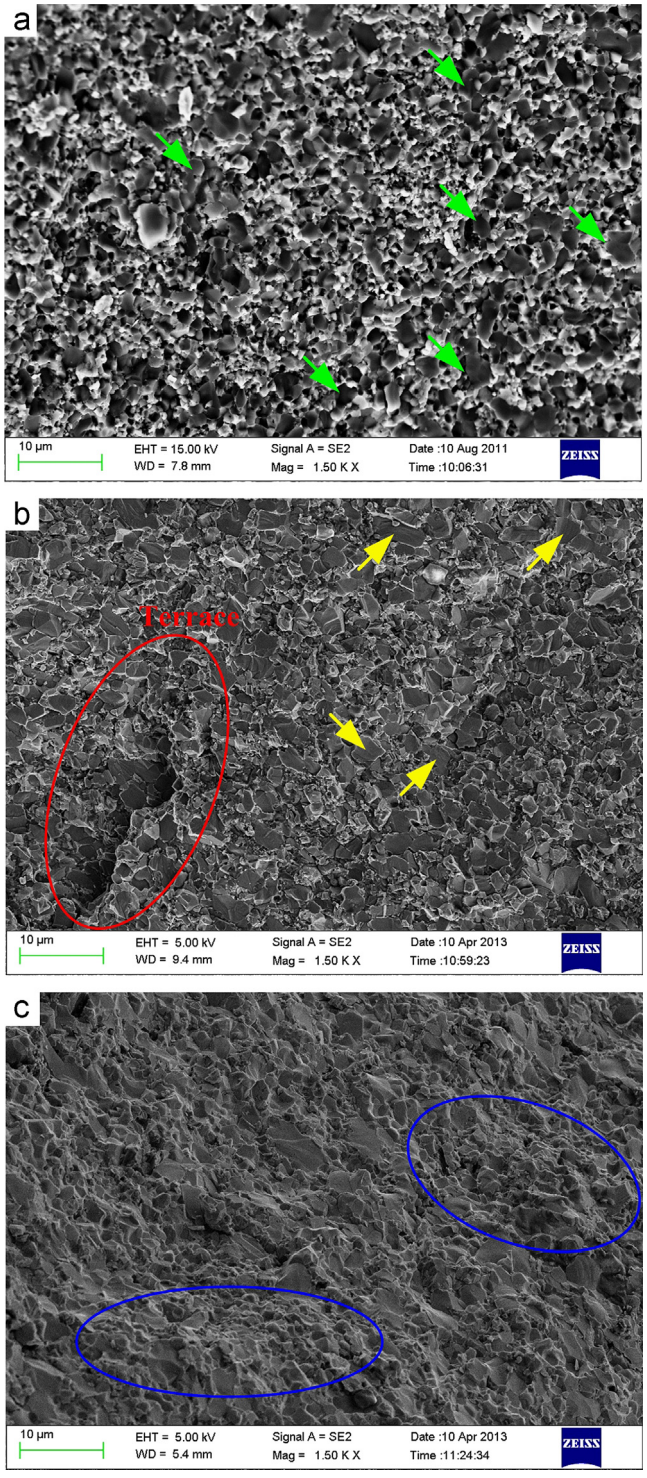

Fig. 6. SEM micrographs of fracture surfaces of the (a) TiB_2–TiC, (b) TiB_2–TiC + Al_2O_3 and (c) TiB_2–TiC + Al_2O_3 + NbC composite materials. The green arrows in (a) indicate the escaped grains along the grain boundaries. The yellow arrows in (b) indicate the cleaving grains, and the red circle indicates the terrace. The blue circles in (c) indicate several plastic deformations. (For interpretation of the references to colour in this figure legend, the reader is referred to the web version of this article.)

the flexural strength of the composite. The TiB_2–TiC + Al_2O_3 + NbC composite material had the highest flexural strength among these three composite materials at 600 °C,

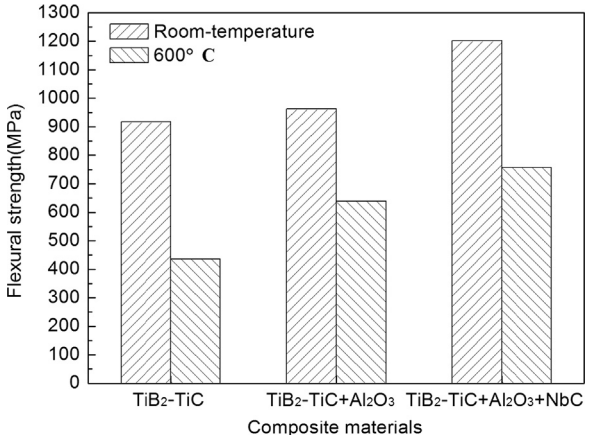

Fig. 7. The flexural strength of the TiB_2–TiC, TiB_2–TiC + Al_2O_3 and TiB_2–TiC + Al_2O_3 + NbC composite materials at room temperature and at 600 °C.

indicating that the superfine NbC additive strengthened the high-temperature flexural strength of the composite. The SEM micrographs of fracture surfaces of the TiB_2–TiC, TiB_2–TiC + Al_2O_3 and TiB_2–TiC + Al_2O_3 + NbC composite materials that failed at 600 °C are shown in Fig. 8. Several cavities were found on the TiB_2–TiC composite material, which indicated that some grains exited the boundary because the Ni binder phase softened at the high temperature. The TiB_2 grains exhibited the transcrystalline rupture, and both the TiC and Al_2O_3 grains exhibited intercrystalline rupture on the TiB_2–TiC + Al_2O_3 composite material. The softening resistance of the TiB_2–TiC was inferior to that of the TiB_2–TiC + Al_2O_3 composite materials, because the Al_2O_3 additive showed a characteristic thermal insulation that could decelerate the softening of the Ni binder phase. Several titanium oxides were found on the fractured surfaces, because these fractured surfaces were exposed to air during cooling. The Al_2O_3 additive improved the oxidation resistance of the composite, which resulted in many more titanium oxides on the fractured surface of the TiB_2–TiC composite material. Much of the Ni binder phase between the grain boundaries was still bonded to the grains on the TiB_2–TiC + Al_2O_3 + NbC composite material. This distributing mode was not observed in the TiB_2–TiC and TiB_2–TiC + Al_2O_3 composite materials, which indicates that the homogenous Ni binder phase and Al_2O_3 additive contributed to the improvement of the flexural strength of the composite. The NbC additive ameliorated the wettability of the Ni liquid phase and caused the Ni binder phase to be more homogeneously distributed. Furthermore, the Al_2O_3 additive retarded the heat transmission, which prevented the Ni binder phase from softening.

Because the flexural strength of the TiB_2–TiC + Al_2O_3 + NbC composite material was high at room temperature, its high-temperature flexural strength was thoroughly investigated. The effects of temperature on the flexural strength of the composite are shown in Fig. 9. The flexural strength of the TiB_2–TiC + Al_2O_3 + NbC composite material decreased as the temperature increased from room temperature to 1000 °C in air. Temperatures above 800 °C more rapidly degraded the flexural

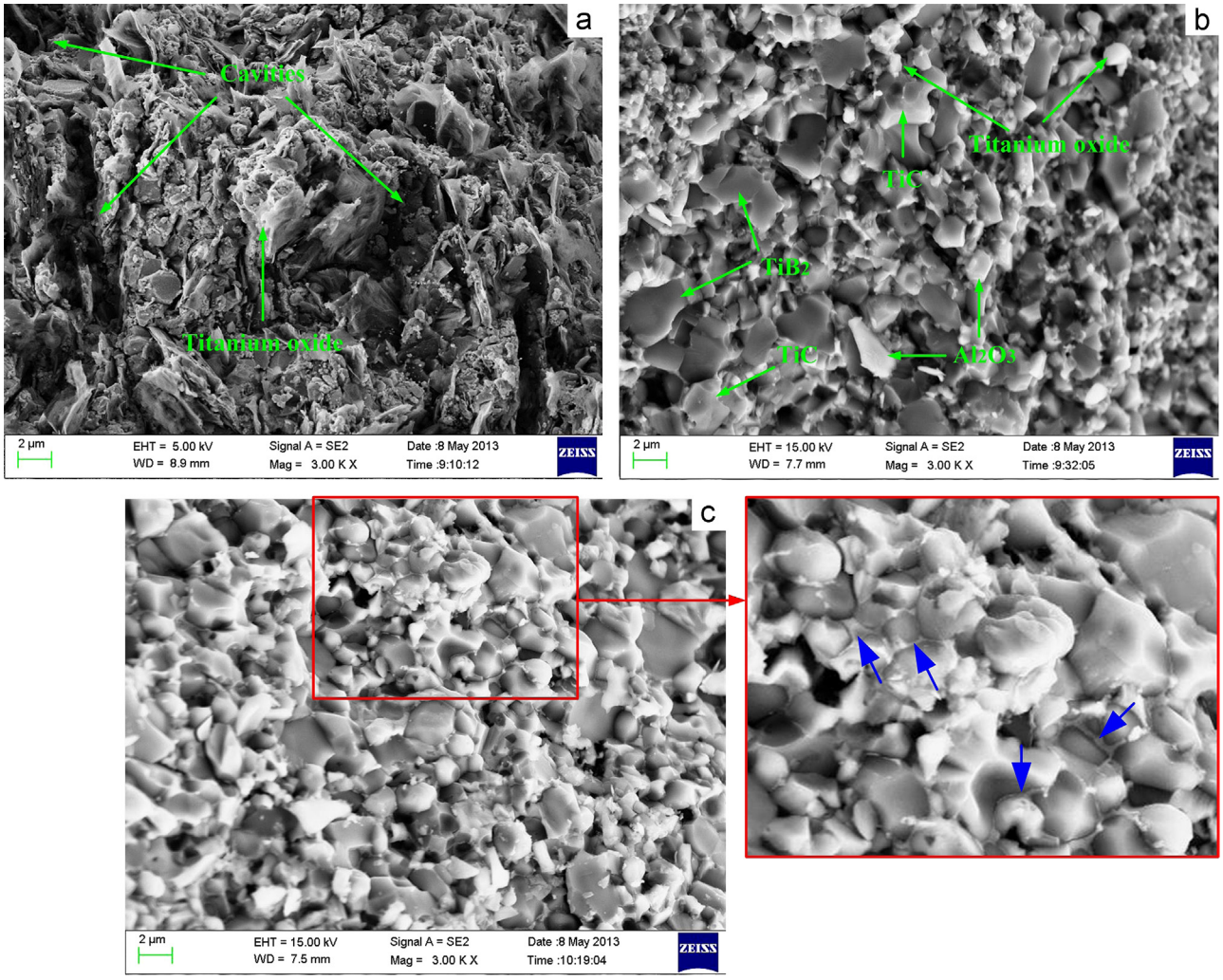

Fig. 8. SEM micrographs of fracture surfaces of the (a) TiB_2–TiC, (b) TiB_2–TiC + Al_2O_3 and (c) TiB_2–TiC + Al_2O_3 + NbC composite materials failing at 600 °C in air.

strength of the composite. When the temperature was increased from room temperature to 600 °C, the flexural strength reduced by approximately 50 MPa for every 100 °C increase. The flexural strength was reduced by approximately 100 MPa per 100 °C from 600 to 800 °C, and the flexural strength decreased by approximately 250 MPa per 100 °C from 800 to 1000 °C. Raju et al. [8] reported an increase in the flexural strength of the TiB_2 + $MoSi_2$ composite material when the temperature was increased from room temperature to 1000 °C. However, a similar result was not found in our work. The flexural strength of the composite fabricated by Raju et al. [8] was only 391 MPa at room temperature and rose slightly to 442 MPa at 500 °C. Thus, the flexural strength of the previously reported material was significantly lower than that of the TiB_2–TiC + Al_2O_3 + NbC composite material below 600 °C, while the flexural strength of the TiB_2–TiC + Al_2O_3 + NbC material was inferior to that of the TiB_2 + $MoSi_2$ composite material at 1000 °C. Cutting tool materials chiefly require a high room temperature flexural strength, because this property can ensure the shock resistance of the cutting tools during machining. More importantly, the flexural strength of the TiB_2–TiC + Al_2O_3 + NbC composite material at 800 °C still exceeded 500 MPa, which can meet the demands of high-speed machining because most of the steel work pieces have already completely softened at this time.

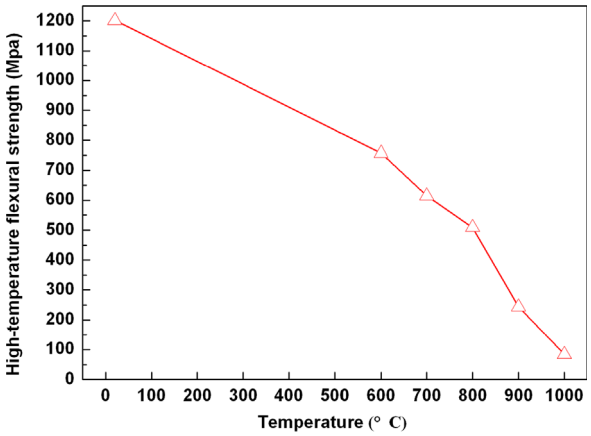

Fig. 9. Change in the high-temperature flexural strength of TiB_2–TiC + Al_2O_3 + NbC composite material as a function of the temperature.

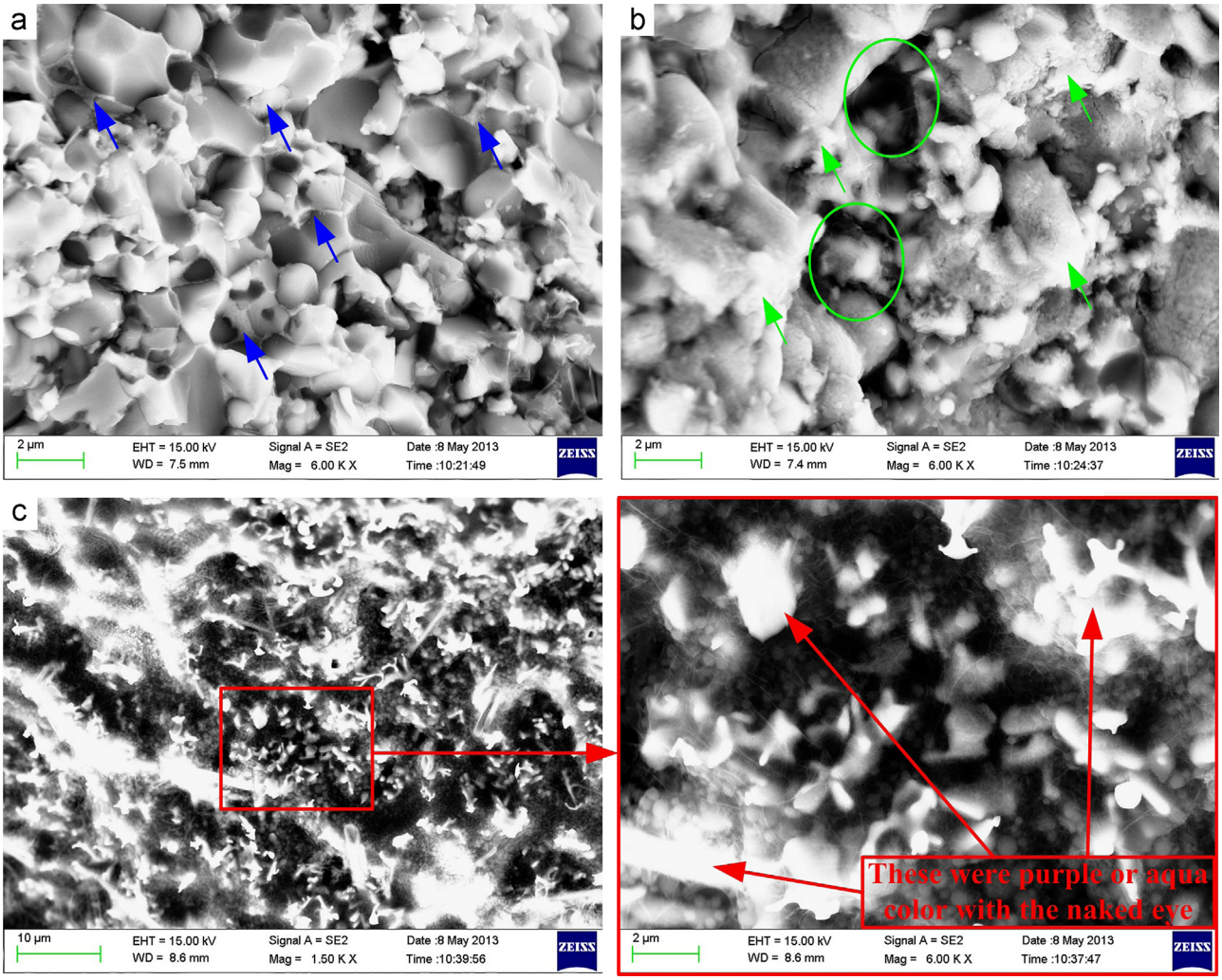

Fig. 10. SEM micrographs of the fracture surfaces of the TiB_2–$TiC+Al_2O_3+NbC$ composite material that failed at (a) 600 °C, (b) 800 °C and (c) 1000 °C in air. (For interpretation of the references to colour in this figure, the reader is referred to the web version of this article.)

The degradation of the high-temperature flexural strength of the TiB_2–$TiC+Al_2O_3+NbC$ composite material was related to the Ni binder phase. Fig. 10 shows the SEM micrographs of fracture surfaces of the TiB_2–$TiC+Al_2O_3+NbC$ composite materials that failed at 600, 800 and 1000 °C in air. The fracture surface of the composite failing at 600 °C was slightly different from that observed at room temperature. Because the Ni binder phase was homogenously distributed on the grain boundaries in the composite, they efficiently prevented the grains from being separated at room temperature. The fracture surface of the composite that failed at room temperature exhibited several plastic deformations, while these plastic deformations almost disappeared due to the softening of the Ni binder phase at 600 °C. However, the bonding strength of the Ni binder phase was not entirely lost at this temperature (see the blue arrows in Fig. 10(a)). The flexural strength of the composite at 800 °C still retained two-fifths of the room temperature flexural strength. Several big cavities remained on the fracture surface at 800 °C (see the green circles in Fig. 10(b)), which indicated that many grains exited when the composite fractured. In addition, the fracture surface contacted some of the Ni binder phase because of the fluidity of the Ni binder phase at 800 °C (see the green arrows in Fig. 10(b)). The fracture surface was obscured and covered by a white substance at 1000 °C (see Fig. 10(c)), which appeared purple or aqua to the naked eye. Ti_2O_3 and NiO_2 appear purple and aqua, respectively, which indicates that the fracture surface was heavily oxidised. However, these oxides were generated predominantly after the sample failed. Because the high-temperature flexural tests required a long time to cool in air, the fracture surfaces of specimens necessarily oxidised.

To investigate the detailed failure mechanism of the TiB_2–$TiC+Al_2O_3+NbC$ composite material at 1000 °C, the morphology of the fracture surface was observed from the side. Fig. 11 shows the SEM micrographs of the polished surface of the $TiC+Al_2O_3+NbC$ composite material that failed at 1000 °C in air, and the fracture surface was viewed from the side of the polished surface. The fracture surface included two smaller terraces (see Fig. 11(b)). The upper terrace belonged to the side of the polished surface, which was adjacent to the

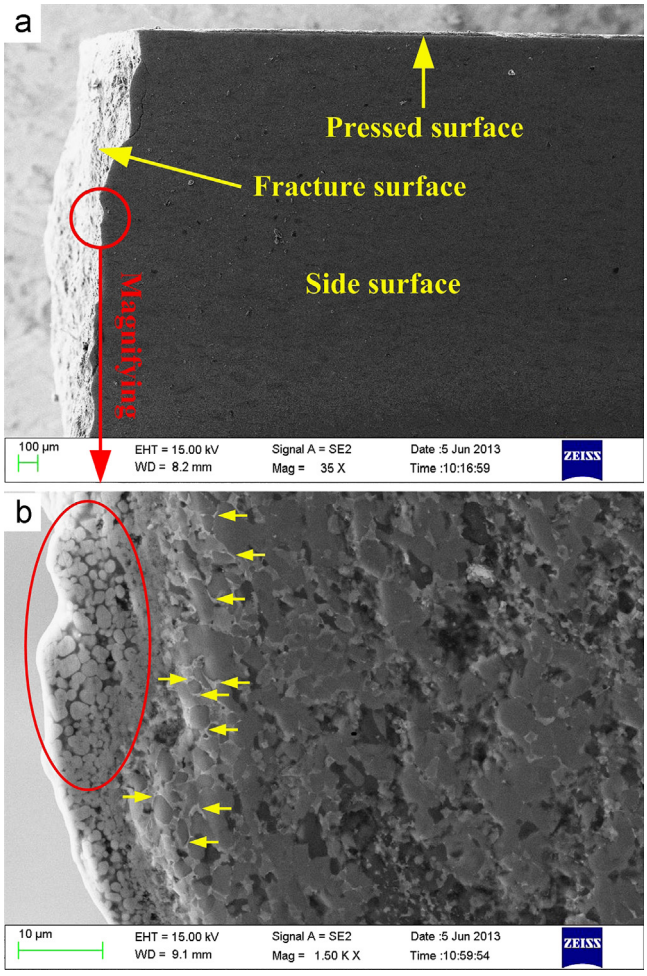

Fig. 11. SEM micrographs of fracture surfaces of the TiB_2–$TiC+Al_2O_3+NbC$ composite material that failed at 1000 °C. The fracture surface was viewed from the side of the polished surface. (For interpretation of the references to colour in this figure legend, the reader is referred to the web version of this article.)

fracture surface, and the lower terrace belonged to the fracture surface. On the upper terrace, the distribution of Ni binder phase was changed on the grain boundaries (indicated by the yellow arrows in Fig. 11(b)), and the average thickness of this Ni binder phase was approximately 70 nm, which was thicker than that observed in the STEM micrograph (see Fig. 5). On the lower terrace, many grains were rounded, and a Ni binder phase was not evident among these grains (see the red circle in Fig. 11(b)). The degradation of the flexural strength of the composite above 800 °C was closely related to the softening of the Ni binder phase. The Ni binder phase had been fluid at 1000 °C in air. Thus, the Ni binder phase was stretched when the composite was under tension. Therefore, the Ni binder phase among the grain boundaries thickened on the side of the polished surface. At this point, some of the Ni binder phase that remained on the fracture surface was oxidised. Because these oxides were easily removed by polishing the side surface, the morphology of the lower terrace was exposed (see the red circle in Fig. 11(b)). These findings explained the decrease in the flexural strength of the TiB_2–$TiC+Al_2O_3+NbC$ composite material at 1000 °C in air.

4. Conclusion

1) The Al_2O_3 additive inhibited the aggregation of TiC grains in the TiB_2–$TiC+Al_2O_3$ composite material while increasing the size of TiB_2 grains. The dispersion of TiC grains benefitted the mechanical properties, while the larger TiB_2 grains adversely affected the mechanical properties. Thus, the TiB_2–$TiC+Al_2O_3$ material showed only slightly higher mechanical properties relative to the TiB_2–TiC material. However, the high-temperature flexural strength of the TiB_2–$TiC+Al_2O_3$ material was significantly higher than that of the TiB_2–TiC material. The Al_2O_3 additive could inhibit the heat transmission in the composite due to its thermal insulation capabilities at high temperatures. The improvement in the high-temperature flexural strength of the TiB_2–$TiC+Al_2O_3$ composite material was primarily attributed to this insulation.
2) When the Al_2O_3 and NbC additives were added together, the aggregation of TiC grains was inhibited and the TiB_2 grains were refined. Most of the Nb entered the TiC and TiB_2 phases during sintering, which resulted in favourable mechanical properties of the TiB_2–$TiC+Al_2O_3+NbC$ composite material (a flexural strength of 1202 MPa, fracture toughness of 8.13 MPa $m^{1/2}$ and hardness of 20.73 GPa). In particular, the addition of NbC improved the flexural strength of the composite by approximately 30%. The addition of NbC resulted in a more homogeneous distribution of the Ni binder phase, which could prevent the grains from being drawn and generating plastic deformations. The improvement of the mechanical properties of the composite is ascribed to the refinement of the microstructure and homogenous distribution of Ni binder phase.
3) The flexural strength of the composite decreased when the temperature increased from room temperature to 1000 °C in air. The plastic deformation on the fracture surface almost disappeared due to the softening of Ni binder phase at 600 °C, while the bonding strength of the Ni binder phase remained high at this temperature. The flexural strength of the TiB_2–$TiC+Al_2O_3+NbC$ composite material at 800 °C was still exceeded 500 MPa, which could meet the demands of high-speed machining. The degradation of the flexural strength of the composite above 800 °C was closely related to the softening of the Ni binder phase. The Ni binder phase became fluid at 1000 °C in air and its bonding strength was almost lost.

Acknowledgements

This project was supported by the National Natural Science Foundation of China (No. 51005136) and the Promotive Research Fund for Excellent Young and Middle-Aged Researchers of Shandong Province (BS2010ZZ005)

References

[1] M.C. Shaw, Metal Cutting Principle, second ed., Oxford University, New York, 2005.

[2] D. Vallauri, I.C. Adrian, A. Chrysanthou, TiC–TiB_2 composites: a review of phase relationships, processing and properties, Journal European Ceramic Society 28 (2008) 1697–1713.
[3] M.L. Gu, C.Z. Huang, S.R. Xiao, H.L. Liu, Improvement in mechanical properties of TiB_2 ceramics tool materials by the dispersion of Al_2O_3 particles, Material Science and Engineering A 486 (2008) 167–170.
[4] B.L. Zou, P. Shen, X.Q. Cao, Q.C. Jiang, Reaction path of the synthesis of α-Al_2O_3–TiC–TiB_2 in an Al–TiO_2–B_4C system, International Journal Refractory Metals and Hard Materials 29 (2011) 591–595.
[5] B. Zou, C.C. Huang, J.P. Song, Effects of sintering processes on mechanical properties and microstructure of TiB2–TiC + 8 wt% nano-Ni composite ceramic cutting tool material, Material Science and Engineering A 540 (2012) 235–244.
[6] B. Zou, C.C. Huang, J.P. Song, Mechanical properties and microstructure of TiB_2–TiC composite ceramic cutting tool material, International Journal Refractory Metals and Hard Materials 35 (2012) 1–9.
[7] J. Wang, Y. Liu, Y. Feng, Effect of NbC on the microstructure and sinterability of Ti(C0.7, N0.3)-based cermets, International Journal Refractory Metals and Hard Materials 27 (2009) 549–551.
[8] G.B. Raju, A. Mukhopadhyay, K. Biswasb, Densification and high-temperature mechanical properties of hot pressed TiB_2–(0–10 wt.%) $MoSi_2$ composites, Scripta Materialia 61 (2009) 674–677.
[9] Z.B. Yin, C.Z. Huang, B. Zou, High temperature properties of Al_2O_3/TiC micro–nano-composite ceramic tool materials, Ceramic International 39 (2013) 8877–8883.
[10] A.G. Evans, E.A. Charles, Fracture toughness determinations by indentation, Journal American Ceramic Society 59 (1976) 371–372.
[11] Y.H. Liu, P.A. Liu, Mechanism and application of X-ray diffraction, first ed., Chemical Industry Press, Beijing, 2011.